J Mater Sci (2014) 49:7462–7475
DOI 10.1007/s10853-014-8451-5

Carbonization behavior of oxidized viscose rayon fibers in the presence of boric acid–phosphoric acid impregnation

Ismail Karacan · Abdullah Gül

Received: 23 April 2014 / Accepted: 5 July 2014 / Published online: 24 July 2014
© Springer Science+Business Media New York 2014

Abstract The oxidation and carbonization stages of viscose rayon fibers were performed in the presence of 3 % phosphoric acid and 4 % boric acid (PA–BA) impregnation. The results showed that PA–BA impregnation enhanced thermal stability and prevented the evolution of volatile by-products. During the oxidation stage carried out at 250 °C, the cellulose II crystalline structure was totally lost due to the decrystallization process. Carbonization was carried out in a pure nitrogen atmosphere at temperatures ranging from 600 to 1000 °C. The results obtained from the fiber thickness, linear density, carbon fiber yield, elemental analysis, volume density, X-ray diffraction, infrared (IR) and Raman spectroscopy, tensile testing, and electrical conductivity measurements showed that the carbonization temperature had a significant effect on the structure and properties of the resulting carbon fibers. Carbon fibers obtained from the oxidized viscose rayon fibers showed physical and chemical transformations with increasing carbonization temperature and were characterized by a reduction in fiber thickness and linear density values due to the removal of non-carbon elements together with increases in the carbon content, carbon to hydrogen ratio (C/H), volume density, tensile strength, tensile modulus, and electrical conductivity values. X-ray diffraction analysis showed that the interplanar *d*-spacing (d_{002}) decreased, and that the apparent crystallite thickness (L_c) and the apparent crystallite width (L_a) increased with increasing temperature. IR spectroscopy in agreement with the elemental analysis showed the total loss of OH, CH, C=O, CH_2, C–O, and C–O–C groups arising from the completion of dehydration and dehydrogenation reactions indicating total elimination of the cellulose structure and the formation of amorphous carbon during high temperature treatment.

I. Karacan (✉) · A. Gül
Department of Textile Engineering, Erciyes University, Kayseri, Turkey
e-mail: ismailkaracanxxx@gmail.com

Introduction

Cellulose fibers are now well established as precursor materials for carbon fiber production with a history dating back to 1880 when Thomas Edison produced the first cellulose-based carbon fiber to be used as an electrical light-bulb filament using cotton and bamboo fibers [1]. His cellulose-based carbon fiber was subsequently used in the 1880s in the electrical illumination of the city of Berlin in Germany [2].

Researchers in England [3], the USA [4], and Japan [5] made considerable research and development efforts to manufacture carbon fibers with desirable properties back in the 1950s and 1960s. The first commercially available carbon fiber was manufactured in the 1950s using regenerated cellulose fibers available in the form of continuous filament bundles for the reinforcement of ablative components for rockets and high temperature missile applications [6].

Apart from regenerated cellulose, carbon fibers can also be produced using precursors such as polyacrylonitrile (PAN) and pitch. Although, historically speaking, cellulose-based carbon fibers were first produced in the 1950s, applications are reported to be limited due to their low tensile strength, low tensile modulus and low carbon yield characteristics [7].

However, as a carbon fiber precursor, regenerated cellulose fibers have major advantages in terms of low cost, high purity (low alkaline metal ion content), high elongation at break, ease of production, ready availability, and renewability characteristics [8].

Natural cellulose fibers, such as cotton, flax, and ramie, are not suitable as precursors of carbon fibers, because of their discontinuous filament structure, low degree of molecular orientation, and the presence of impurities such as lignin and hemicellulose [9].

Most commercially produced PAN- and pitch-based carbon fibers are not suitable for missile heat shielding and ablative applications due to their low purity (high alkaline metal content), high thermal conductivity, and high axial and/or transverse thermal expansion coefficients [10].

To meet the demands posed by the rapid development of aerospace, transportation, and medical applications, scientists are once again concentrating on cellulose-based carbon fibers in order to take full advantage of their desirable properties including low thermal conductivity, low density, high purity (low alkaline metal content), high elongation at break, and high flexibility characteristics [10]. It has now been clearly established that the low thermal conductivity of cellulose-based carbon fibers is due to the presence of a highly disordered graphitic structure (i.e., turbostratic). Carbon fibers containing a turbostratic structure are generally characterized by excellent thermal insulation and ablation resistance properties. Regenerated cellulose-based carbon fibers have been considerably utilized in special fields, such as aerospace, aviation, and other high technology areas as structural reinforcement material, especially for heat protection in missiles, rocket motor casings, and jet engine parts [11–14].

Furthermore, regenerated cellulose-based carbon fibers are reported to have good blood compatibility which means they can be used in medical treatments [11]. Regenerated cellulose fibers are also nowadays used for the production of activated carbon fibers (ACF) [15]. ACFs play an important role in both industrial and medical applications, including the preparation of high quality drinking water, waste water treatment, gas separation for industrial applications, hemodialyzers, and the controlled release of drugs [16]. ACFs in the form of woven, knitted, and non-woven fabric are often utilized for the removal of pollutants such as pesticides [17, 18] from waste water by adsorption processes. ACFs are also used for metal ion adsorption [19], electromagnetic interference shielding [20], as electrodes for high-performance electric double-layer capacitors [21], for noise absorption [22], noise insulation [23], methane [24] and hydrogen gas storage [25], and in the manufacture of personal protective suits [26].

Most cellulose-based carbon fibers are produced from textile-grade rayon or viscose rayon multifilament yarns [11, 27]. Also, other regenerated cellulose fibers including saponified acetate rayon, cuprammonium rayon, polynosic rayon, Lyocell and recently introduced Bocell have also been used as precursors in the production of carbon fibers [7, 10, 11, 28].

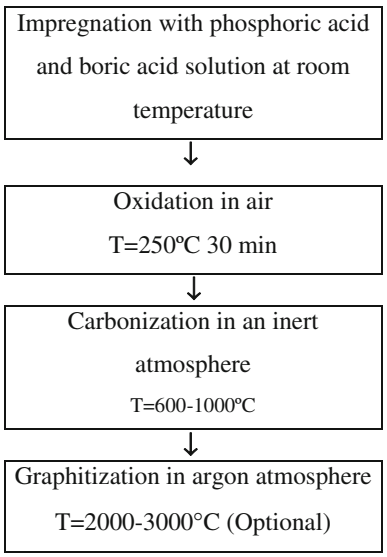


Fig. 1 Viscose rayon-based carbon fiber production flow chart

On a commercial scale, cellulose-based carbon fibers are produced by Rue-Spa Khimvolokno (Belarus), and by SGL Carbon (Germany). Recently, Lenzing AG of Austria announced plans to produce cellulose-based carbon fibers on a commercial scale [9, 29].

Highly crystalline natural cellulose precursor fibers (bacterial, algal, tunicate, and ramie) have also been used recently in the production of cellulose-based carbon fibers [30–32]. In a recent publication, cotton-based carbon fiber was reported to have been used for hydrogen storage after nickel and iron nitrate impregnation followed by a slow carbonization process [33]. Cellulose-based carbon fiber is manufactured using a series of steps consisting of impregnation with chemicals, oxidative stabilization (i.e., thermal stabilization) in air, and carbonization in an inert atmosphere (Fig. 1). The thermal stabilization step is normally performed in air at temperatures ranging from 200 to 300 °C and is a necessary step to prevent the precursor fibers from degradation during the subsequent carbonization [34]. Carbonization is normally carried out at up to 1300 °C for up to 1.5 h in the presence of an inert atmosphere [13, 35]. The carbonization stage may be followed by an optional stage of graphitization (Fig. 1) [12]. During the graphitization step, higher carbon content and higher tensile modulus values can be reached provided certain conditions are met [36].

The aim of the present investigation was to study the carbonization behavior of oxidized viscose rayon fibers impregnated with a boric acid (BA)–phosphoric acid (PA) solution. The structural characterization of carbonized samples was with the aim of monitoring and following the structural transformations taking place as a function of carbonization temperature.

Experimental details

Preparation of oxidized and carbonized samples

Untreated viscose rayon multifilament yarn with a linear density of 32.6 tex per 64 filaments was used. Untreated viscose rayon multifilament yarn was treated with a 5 % (v/v) aqueous ethanol solution for 30 min at 50 °C to remove the impurities present on the surface of the fibers followed by a thorough washing under running water for 30 min to remove the final remains. Chemical impregnation was carried out by immersing the samples in a 3 % (w/v) PA and 4 % (w/v) BA combination at room temperature for 30 min. The solution had a pH value of 1.51 at 24 °C. BA (99.9 % purity) and PA (85 % conc.) were obtained from Kimetsan AS (Ankara, Turkey). Following the immersion of the samples, each sample was taken out and the excess solution was removed by a towel and dried at 50 °C for 24 h. The pretreated viscose rayon contained 8.6 % (w/w) PA and BA on a dry basis. Oxidation was subsequently carried out in air at 250 °C for 30 min. The samples were originally wound onto stainless steel frames with the aim of constraining them to prevent physical shrinkage and also to prevent the loss of molecular orientation. Oxidative thermal stabilization was carried out with a heating rate of 1 °C/min.

Carbonization was carried out in a tubular furnace designed to work up to 1200 °C. The oxidized sample was wound onto a specially made sample holder before positioning in the middle of the furnace. Nitrogen gas was allowed to flow at least 2 h before the carbonization process. Under normal circumstances the nitrogen gas flow rate was 150 mL/min. During the carbonization experiments a heating rate of 2 °C/min was employed. Carbonization was carried out at temperatures between 600 and 1000 °C in steps of 100 °C for a residence time of 30 min in each case.

Experimental data collection

The fiber thickness of the oxidized and carbonized fibers was evaluated using a polarizing microscope (Nikon ME600L, Japan) with a calibrated eyepiece.

Linear density was determined by measuring the weight in grams per unit length of a multifilament bundle. In the present investigation, tex is used as a linear density which is defined as the weight of a multifilament bundle in grams per 1000 m.

Density values were evaluated using a density gradient column operating at 23 ± 1 °C. The column was prepared using perchloroethylene ($\rho = 1.61$ g/cm^3) and isopropyl alcohol ($\rho = 0.77$ g/cm^3) for the measurement of the density of the original viscose rayon fiber, the sample oxidized at 250 °C for 30 min and the samples carbonized at 600 and 700 °C. In the case of the fiber samples carbonized between 800 and 1000 °C, the column was prepared using zinc chloride ($\rho = 2.91$ g/cm^3) and water. The samples were allowed approximately 24 h to reach their equilibrium level of displacement. The density gradient column was calibrated by adding a set of known density floats and plotting a graph of the density of the floats versus the height at which each calibrated float settled after 24 h in the column.

Chemical elemental analysis for C, H, and C/H ratio was carried out by combustion in a LECO® TruSpec Micro Elemental Analyzer (Leco Corp., USA). For oxidized and carbonized samples, high temperature combustion was used as the means of removing elements from the material. In the combustion process, the sample was encapsulated in a tin capsule with an average weight of 2 mg. The sample was placed in the sample loading chamber and held there until a dose of oxygen was released. It was then dropped into the furnace. The sample was combusted in the heated, oxygen-rich environment. Calibration was performed with benzoic acid for the carbon and hydrogen content calibrations.

The wide-angle X-ray diffraction traces were obtained using a Bruker® AXS D8 Advance X-ray diffractometer system utilizing nickel-filtered CuK_α radiation (wavelength of 0.15406 nm) and voltage and current settings of 40 kV and 40 mA, respectively. Counting was carried out at 10 steps per degree. The observed equatorial X-ray scattering data were collected in reflection mode in the 5–35 and 35–55° 2θ range, respectively. The collected X-ray diffraction data were corrected for Lorentz and polarization factors [37].

A Perkin Elmer® Spectrum 400 FT-IR spectrometer was employed for infrared measurements using a single reflection diamond-based GladiATR® model ATR attachment in absorbance mode. In all cases, 50 interferograms of sample were averaged and transformed with a medium Norton–Beer apodization function. Each sample spectrum was ratioed against a corresponding number of background scans using the same instrument settings. A 2/cm resolution and 4000–400/cm mid-IR range was used throughout the experiments.

Raman scattering studies were conducted on a Renishaw InVia Raman microscope equipped with an excitation wavelength of 785 nm (Diode laser). The Raman microscope delivers 60 mW power to the sample and is equipped with a Peltier-cooled CCD detector (576 × 288 pixels) operating at −70 °C. All measurements were made in a backscattering geometry using a 50× microscope objective with an NA value of 0.75, providing scattering areas of ~1 μm^2. Samples were scanned using a Renishaw

SynchroScan mode from 2000 to 500/cm with a spectral resolution of 2/cm. The spatial resolution achieved was up to 1 μm, depending on the set parameters. The number of acquisitions varied and signals were accumulated to improve the signal-to-noise ratio [38].

The tensile properties of the carbonized samples were obtained using a PROSER tensile tester at room temperature. Tensile testing of the carbonized samples was carried out using a gage length of 10 mm and a crosshead speed of 1 mm/min. Careful attention was paid to minimize slippage of the multifilaments during testing. Due to the brittle nature of the carbonized samples, single filaments were difficult to separate, hence, multifilament bundle was used for the tensile testing measurements. Tensile properties in terms of tensile strength and tensile modulus were first obtained in N/Tex. Finally, the tensile properties were converted to GPa by multiplying N/Tex with the density values in g/cm^3. Tensile modulus was evaluated from the initial slope of the tensile curve. The elongation and tensile strength at break were determined at the position of break. Reported values were the averages of at least 20 tests.

All the electrical measurements of the samples were obtained by the DC four-point probe method. This method is the most widely used technique for electrical profile measurements of materials and has been proven to be a convenient tool for the resistivity measurements. A four-point probe measurement is performed by placing four electrical probes onto the sample surface. Two of the probes are used to supply current and the other two probes are used in measuring voltage. The advantage of using four probes is that this eliminates the measurement errors due to probe resistance, the spreading resistance under each probe, and the contact resistance between each metal probe and the material [39, 40].

A Keithley 2400 sourceMeter was utilized to provide the constant current, and the potential drop was measured by a Keithley 2700 multimeter through an interface card, both controlled by a computer. Platinum wires of 0.5 mm diameter were employed as current and potential electrodes. The voltage drop was detected, and the electrical resistivity and conductivity were obtained using a standard conversion method. The measurements were carried out at room temperature [40]. At least 15 samples were tested to determine the average electrical properties.

Experimental data analysis

X-ray data-curve fitting

All the X-ray diffraction traces obtained from the oxidized and carbonized samples were fitted with a curve fitting procedure developed by Hindeleh et al. [37] to separate the overlapping peaks. Curve fitting of the equatorial X-ray diffraction traces was carried out with a linear baseline. The region below the baseline is attributed to an instrumental background signal which may include air and incoherent scattering.

Evaluation of apparent crystallite size

The peak widths at half-height were corrected using the Stoke's deconvolution procedure [41]. Then the apparent crystallite size, for a given reflection, was calculated using the Scherrer equation (1) as follows:

$$L(hkl) = \frac{K.\lambda}{\beta.\cos(\theta)}, \quad (1)$$

where θ is the Bragg angle for the reflection concerned, λ is the wavelength of the radiation (wavelength of 0.154056 nm), $L(hkl)$ is the mean length of the crystallite perpendicular to the planes (hkl), β is either the integral breadth or the breadth at half maximum intensity in radians, and K is a Scherrer parameter usually taken as 1 for integral breadths and 0.89 for half-widths. Hexamethylenetetramine compacted at 85 °C, which should have infinite size crystals, was used for the instrumental broadening correction.

Evaluation of porosity

A large amount of voids are introduced during the wet spinning of viscose rayon fibers [11]. The amount of porosity arising from the presence of voids was evaluated [42] using the volume density of the carbon fiber samples and the X-ray density (pure graphite), using Eq. (2) as follows:

$$\text{The porosity } (\%) = \left[1 - \frac{\rho d_{002}}{\rho_g d_g}\right] \times 100, \quad (2)$$

where ρ is the carbon fiber density and d_{002} is the interplanar d-spacing of the carbon fiber. ρ_g is the density of graphite (2.26 g/cm^3) and d_g is the d-spacing of the (002) reflection of graphite (0.3354 nm).

Correction of experimental tensile modulus

Tensile modulus must be corrected from the effects of porosity (ratio of the density of the bulk carbon in the fibers to the macroscopic fiber density) [43, 44]. The values of tensile modulus were corrected for the effects of porosity by assuming that the effect of pores is restricted to a reduction of the effective cross-section of the carbon fibers [43] using Eq. (3) as follows:

Table 1 Properties of oxidized and carbonized viscose rayon fibers pretreated with combined 3 % (w/v) phosphoric acid (H_3PO_4) and 4 % (w/v) boric acid (H_3BO_3) solution as a function of carbonization temperature

Carbonization temp (°C)	Fiber thickness μm	Fiber thickness loss (%)	Linear density (Tex)	Linear density loss (%)	Yield (%)	Density g/cm^3
Untreated	24.0 ± 0.3	0.0	32.6	0.0	–	1.503 ± 0.002
250 °C 30 min	17.9 ± 0.2	25.4	21.6	33.7	66.3	1.455 ± 0.055
600	17.0 ± 0.1	29.2	15.6	52.2	47.8	1.464 ± 0.003
700	15.8 ± 0.1	34.2	14.7	54.9	45.1	1.480 ± 0.003
800	14.1 ± 0.2	41.3	13.3	59.2	40.8	1.584 ± 0.003
900	12.4 ± 0.1	48.3	12.7	61.0	39	1.620 ± 0.005
1000	10.5 ± 0.1	56.3	11.0	66.3	33.7	1.642 ± 0.004

$$E_{\text{corr}} = \frac{\rho_g d_g}{\rho d_{002}} E, \tag{3}$$

where E is the experimental tensile modulus of carbon fibers, ρ is the carbon fiber density, and d_{002} is the interplanar d-spacing of the carbon fiber. ρ_g is the density of graphite (2.26 g/cm^3) and d_g is the d-spacing of the (002) reflection of graphite (0.3354 nm) [44].

Results and discussion

Oxidation in an oxygen-containing atmosphere is a necessary step during the production of regenerated cellulose-based carbon fibers prior to the carbonization and graphitization stages. Oxidative thermal stabilization enables the precursor fibers to resist the high temperatures involved during the carbonization stage. In the present investigation, viscose rayon precursor fiber was impregnated with a 3 % PA and 4 % BA solution prior to oxidative stabilization followed by oxidation in air at 250 °C for 30 min. The PA and BA combination was used as an impregnant for viscose rayon fiber for its good flame retardation effects prior to the oxidation step [45].

The fiber thickness values of the carbon fibers as a function of carbonization temperature are presented in Table 1. The fiber thickness of the oxidized sample with oxidation temperature of 250 °C was reduced to 17.9 μm as compared to 24 μm in the original viscose rayon fiber. The fiber thickness values of the carbon fibers fall off sharply when carbonization treatment at 600 °C and above is performed. The most significant reduction in the fiber thickness was recorded after a carbonization temperature of 1000 °C with approx. 56.3 % loss in fiber thickness (Table 1) which took place with respect to the untreated sample. The main reason for the severe reduction in fiber thickness is due to the weight loss which took place due to the loss of non-carbon elements in the form of volatiles such as H_2O, CO, and CO_2 during the oxidative stabilization and carbonization stages.

Variation in the linear density of the carbonized fiber samples as a function of carbonization temperature is shown in Table 1. The linear density of the carbon fibers was reduced from 32.6 to 11 tex with a corresponding loss of 66.3 % with respect to the untreated viscose rayon fiber when the carbonization temperature was increased from 600 to 1000 °C. The reduction in linear density with carbonization temperature is related to the elimination of water, CO, and CO_2 occurring during the dehydration reactions.

The carbon fiber yields, taking into account the weight changes per unit length through the carbonization steps, are listed in Table 1. The results listed in Table 1 suggest that the carbon fiber yield is 66.3 % for the oxidized sample at 250 °C for 30 min. In the case of the carbonized samples, the carbon fiber yield decreases from 47.8 to 33.7 % with increasing carbonization temperature, which is in agreement with the published literature [5].

Elemental analysis

Elemental analysis was carried out to determine quantitatively the change in concentration of carbon and hydrogen elements and carbon to hydrogen (C/H) ratio as a function of carbonization temperature. The results of elemental composition analysis of the carbon fibers during the carbonization stage are presented in Fig. 2a–c. The carbon content of the carbon fibers increases gradually from 77.5 to 90.3 % as the carbonization temperature increases, as shown in Fig. 2a, whereas the content of hydrogen and C/H ratio gradually decrease with a rise in carbonization temperature, as shown in Fig. 2b–c. C/H ratio was also found to increase from 31.5 to 143.3 with increasing temperature.

As shown before from the measurements of linear density, weight loss occurs during carbonization. The non-carbon elements are removed as volatiles, such as H_2O, CO, CO_2, and H_2 to give a yield of 33.7 % at 1000 °C (Table 1). At the carbonization temperatures of 600–800 °C, the hydrogen content manifests a rapid reduction, due to extensive dehydrogenation reactions, as

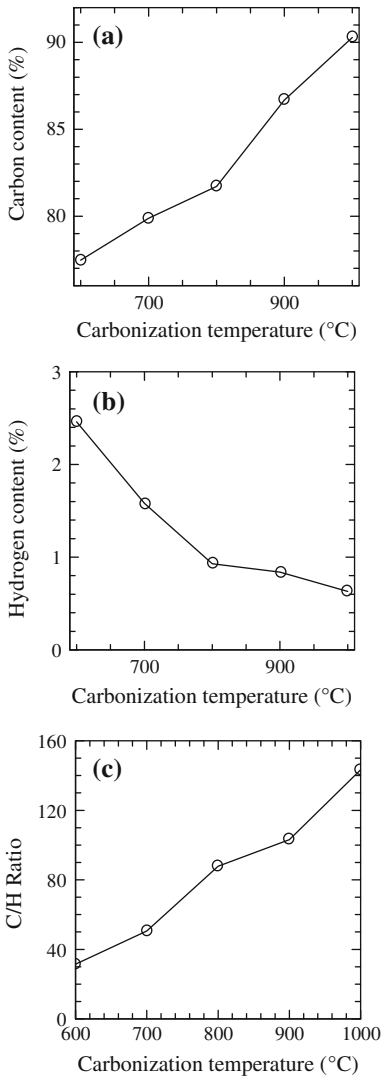


Fig. 2 Elemental composition of carbon fibers **a** carbon content (%), **b** hydrogen content (%), **c** C/H ratio

shown in Fig. 2b. Above the carbonization temperature of 800 °C, the hydrogen content decrease becomes less significant. During carbonization reactions, hydrogen content decreased from 2.5 to 0.6 % when the temperature increased from 600 to 1000 °C.

It is suggested that at the carbonization temperature of 600 °C and above, the ladder polymer chains formed from intramolecularly and intermolecularly crosslinked chains after the oxidation step at 250 °C for 30 min appear to be crosslinked further and lead to the formation of volatiles in the form of H_2O, CO, CO_2, and H_2. This reaction also causes the lengthening, broadening, and thickening of the graphene planes. The formation of such a structure facilitates the formation of more graphene planes, which eventually leads to the enhancement of the tensile properties of the final carbon fibers.

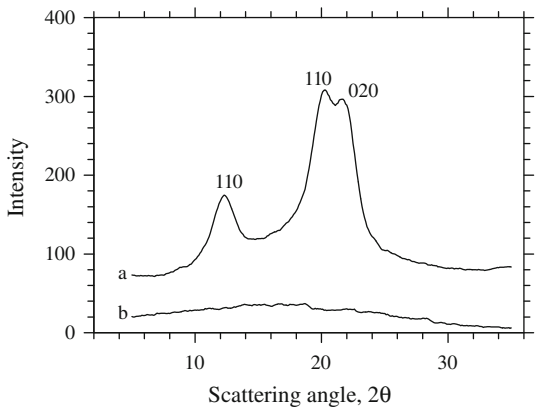


Fig. 3 Equatorial X-ray diffraction traces of untreated (**a**) and combined 3 % phosphoric acid and 4 % boric acid-impregnated viscose rayon fibers oxidized at 250 °C for 30 min (**b**)

Volume density measurements

Table 1 shows the density values of the carbonized fiber samples as a function of carbonization temperature. The density of untreated viscose rayon fiber was determined using a density column to be 1.503 g/cm^3. The density of the sample oxidized at 250 °C for 30 min was found to be 1.455 g/cm^3. The density values of carbonized samples increased from 1.464 to 1.642 g/cm^3 when the carbonization temperature increased from 600 to 1000 °C. The increase with increasing carbonization temperature confirms the development of compaction of the whole structure, possibly due to the development of aromaticity (i.e., cyclization) or extensive cross-links in the structure of the carbonized fibers. The increase in density with progressing temperature is also due to the removal of non-carbon elements from the fibers as a result of the occurrence of aromatization reactions and crosslinking of the heterocyclic rings, as well as to the broadening and lengthening of carbon basal planes.

X-ray diffraction

The equatorial X-ray diffraction traces of untreated viscose rayon fibers and viscose rayon fibers oxidized at 250 °C for 30 min in the presence of PA–BA are presented in Fig. 3. The qualitative examination of the equatorial X-ray diffraction traces of untreated viscose rayon fibers plotted in Fig. 3a shows three crystalline reflections as the most predominant features. The equatorial X-ray diffraction traces of untreated viscose rayon fiber plotted in Fig. 3a can be resolved into three crystalline reflection peaks indexed as the $1\,\bar{1}\,0$, 110, and 020 reflections of a cellulose II structure with *d*-spacings of 0.728, 0.441, and 0.405 nm,

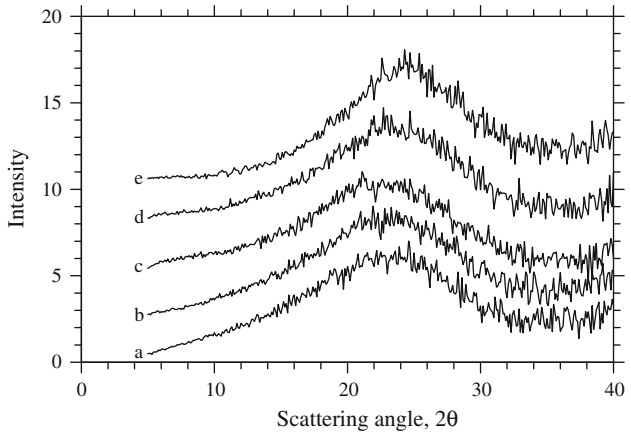


Fig. 4 Equatorial X-ray diffraction traces of carbonized fiber samples as a function of carbonization temperature. **a** 600 °C, **b** 700 °C, **c** 800 °C, **d** 900 °C, **e** 1000 °C

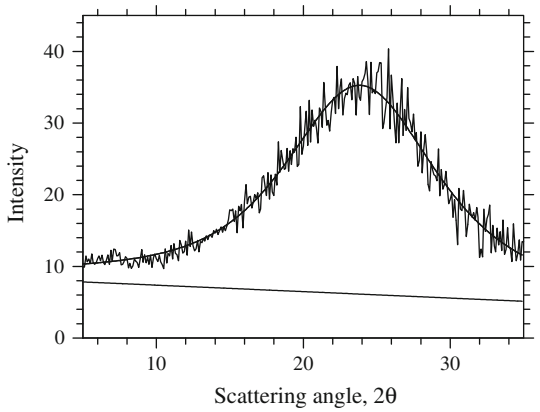


Fig. 5 Curve fitting of equatorial X-ray diffraction trace of carbonized viscose rayon fibers at 1000 °C for 30 min

respectively. These reflections correspond to the monoclinic unit cell [46] dimensions of $a = 0.810$ nm, $b = 0.903$ nm, $c = 1.031$ nm, and $\gamma = 117.1°$.

PA–BA impregnation followed by oxidation in air at 250 °C for 30 min seems to have a considerable influence on the crystal structure of the viscose rayon fibers in terms of the degree of apparent crystallinity. The equatorial X-ray diffraction trace plotted in Fig. 3b demonstrated a total loss of crystallinity. The results demonstrated that a typical decrystallization (i.e., disordering) process seems to be taken place during the oxidation process at 250 °C. The X-ray diffraction trace of the sample oxidized at 250 °C (Fig. 3b) was characterized by a broad halo-like scatter spreading between scattering angles of 5 and 30°.

The equatorial X-ray diffraction traces in the 5–40° 2θ range of carbonized samples are plotted in Fig. 4. The X-ray diffraction traces shown in Fig. 4 are characterized by a broad diffraction peak indicating the presence of amorphous carbon interlayers. The diffraction peak position shifts to higher values and becomes slightly narrower with increasing carbonization temperature indicating the growth of carbon interlayers. These carbon interlayers are similar to graphitic crystallites but are not stacked in any particular sequence; they are known as turbostratic carbon crystallites [47]. The X-ray diffraction traces shown in Fig. 4 are curve fitted to obtain accurate peak parameters in terms of peak position, peak intensity, and half-height width (HHW). A typical curve fitting is presented in Fig. 5 for the sample carbonized at 1000 °C for 30 min.

The values of peak position and HHW were used to evaluate the interplanar *d*-spacing and the apparent crystallite size (in this case crystallite thickness, L_c) using Eq. (1) as shown in Table 2. With increasing carbonization temperature, the diffraction peak position moved from

Table 2 Analysis of equatorial X-ray diffraction traces of carbonized viscose rayon fibers pretreated with combined 3 % (w/v) phosphoric acid (H_3PO_4) and 4 % (w/v) boric acid (H_3BO_3) solution as a function of carbonization temperature

Carbonization temp (°C)	Peak position $(2\theta)_{002}$	*d*-spacing (002) nm	Half-height width (°)	L_c (002) nm	Number of graphene layers (N)
600	22.43	0.396	14.82	0.608	1.5
700	22.56	0.394	14.67	0.614	1.6
800	22.61	0.393	14.38	0.626	1.6
900	23.25	0.382	13.16	0.685	1.8
1000	24.12	0.369	11.49	0.786	2.1

$2\theta = 22.43°$ to 24.12° indicating a decrease of interplanar *d*-spacing from 0.396 to 0.369 nm. It is reported in the literature that the (002) diffraction peak of disordered carbons appears at $2\theta = 22$ to 25° [48, 49]. The main diffraction peak appearing between $2\theta = 22.43°$ to 24.12° associated with the carbonaceous interlayer should be differentiated from the graphitic interlayer [49].

The HHW of the same peak after instrumental correction was used to determine the apparent crystallite thickness (L_c). The results suggest that the crystallite thickness increases from 0.608 to 0.786 nm with increasing carbonization temperature from 600 to 1000 °C. Increasing crystallite thickness (L_c) corresponds to an increase of graphene layers from 1.5 to 2.1 when the carbonization temperature of 1000 °C was reached (Table 2).

The equatorial X-ray diffraction traces of the same carbonized samples were obtained in the 35–55° 2θ range to evaluate the average apparent crystallite width (i.e., in-plane graphene width) (L_a) through the use of the Scherrer equation (1). Curve fitting was also performed for the (100) reflection peak. The results obtained from the curve fitting

Table 3 Resolved peak parameters of curve-fitted equatorial X-ray diffraction trace of carbonized viscose rayon fibers in the 35–55° 2θ range

Carbonization temperature (C)	Profile function parameter	Peak height	Half-height width (2θ)	Peak position (100)	d-obs spacing (nm)	L_a (nm)
600	1.0	2.41	14.58	44.00	0.2056	0.653
700	1.0	3.03	10.22	44.13	0.2050	0.933
800	0.87	2.80	7.981	44.51	0.2034	1.196
900	1.0	2.11	7.935	44.55	0.2032	1.203
1000	1.0	2.80	5.245	44.62	0.2029	1.821

of the (100) reflection suggest that the peak position moved from 44 to 44.62° 2θ with increasing temperature. The corresponding interplanar d-spacing decreased from 0.2056 to 0.2029 nm (Table 3). This peak is often referred to as (100) reflection in fully graphitized samples. The corrected half-height of this peak is used to determine the crystallite width often referred to as L_a in fully developed graphitized structures. The values of L_a increased from 0.653 to 1.821 nm when the carbonization temperature was increased from 600 to 1000 °C (Table 3).

Infrared spectroscopy

During the present investigation, mid-IR spectroscopy was effectively used to follow the structural transformations taking place during the oxidation and carbonization stages. Our earlier study [45] showed a continuous decrease in the intensities of OH and CH vibrations in the region between 4000 and 2800/cm due to the loss of intramolecular and intermolecular hydrogen bonds together with dehydration processes with increasing temperature from 150 to 250 °C. The gradual loss of intermolecular hydrogen bonding during oxidation was attributed to the loss of crystallinity and the formation of an amorphous phase with increasing temperature. The gradual disappearance of the hydrogen-bonded OH groups and hydrogen atoms from the CH groups with increasing temperature was considered to be a clear sign of dehydration and dehydrogenation reactions taking place during the oxidation step.

At the oxidation temperature of 250 °C, the strong and broad band at 1720/cm was attributed to C=O stretching of ketone, aldehyde, lactone, and carboxyl groups [50]; a new band associated with C=C bonds located around 1610/cm appeared as a broad band (Fig. 6).

C=C stretching located at 1610/cm was observed to be predominant in the sample oxidized at 250 °C indicating that oxidized cellulose contained highly aromatic structures (Fig. 6b). The results showed that oxidation in the presence of PA–BA impregnation catalyzed the dehydration reactions. The formation of boron phosphate containing borate and phosphate (BO_4 and PO_4) groups enhanced the dehydration and crosslinking reactions at lower temperatures.

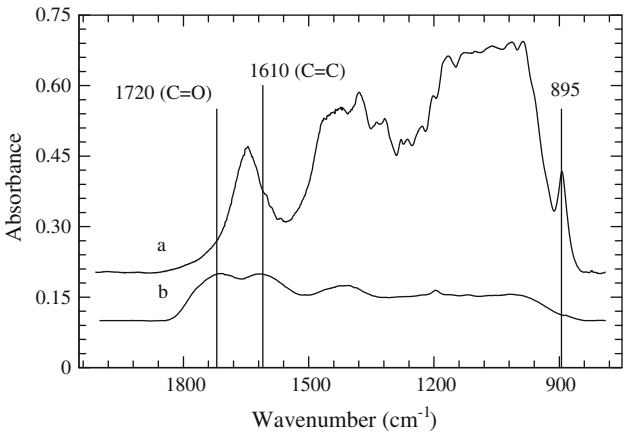


Fig. 6 Infrared spectra of untreated (**a**) and PA–BA-impregnated viscose rayon fibers oxidized in air at 250 °C for 30 min (**b**) in the 1900–800/cm region

Boron phosphate was also found to prevent the formation of volatile substances by blocking the primary hydroxyl groups. The results also indicated the collapse of the basic cellulose structure at 250 °C [45].

After the oxidative stabilization stage, the samples were carbonized from 600 to 1000 °C in steps of 100 °C for 30 min in each case. Carbonizing the oxidized sample (250 °C for 30 min) at 600 °C and above caused the total disappearance of the OH and CH groups in the 4000–2375/cm region due to the completion of dehydration and dehydrogenation reactions (Fig. 7). The intensities of the IR absorption bands corresponding to the carbon fibers in the 1900–800/cm region were found to be extremely weakened and broadened for the carbonized samples presented in Fig. 8. The most noticeable feature in the IR spectra of the carbon fibers in the 1900–800/cm region is the total disappearance of the C=O band at 1720/cm, CH_2 symmetric bending at 1424/cm, C–O stretch bands (1100–975/cm), and C–O–C stretching of the cellulose ring at 875/cm [45] after the carbonization temperature of 600 °C indicating the removal of oxygen and hydrogen elements from the carbonized structure.

The C=C stretching band was found to shift from 1610 to 1560/cm following carbonization in an inert atmosphere

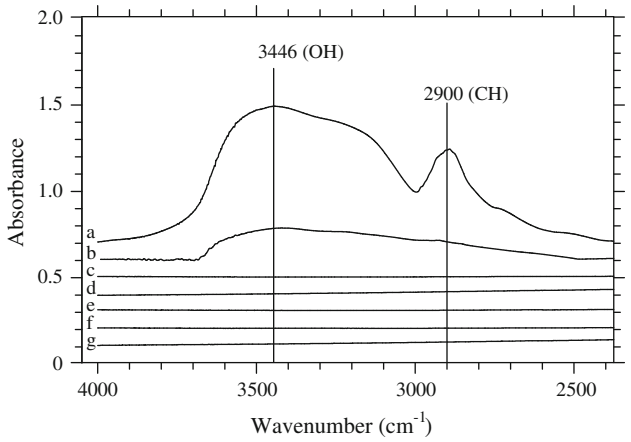


Fig. 7 Infrared spectra of untreated (**a**) and PA–BA-impregnated viscose rayon fibers oxidized in air at 250 °C for 30 min (**b**) and carbon fibers as a function of carbonization temperature in the 4000–2375/cm region. **c** 600 °C, **d** 700 °C, **e** 800 °C, **f** 900 °C, **g** 1000 °C

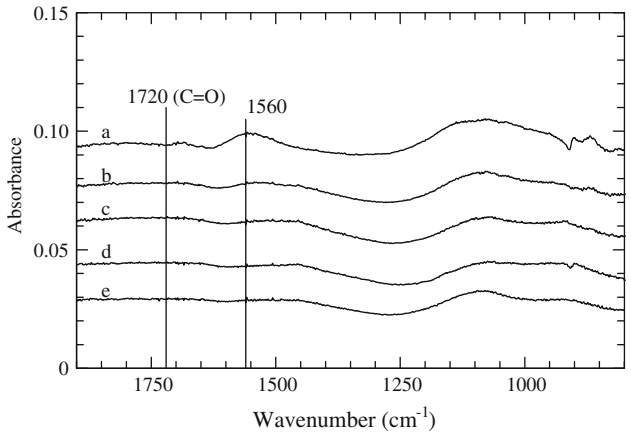


Fig. 8 Infrared spectra of carbon fibers as a function of carbonization temperature in the 1900–800/cm region **a** 600 °C, **b** 700 °C, **c** 800 °C, **d** 900 °C, **e** 1000 °C

in the IR spectra of the carbon fibers (Fig. 8). The results from the analysis of IR spectra suggest that the polymerization of aromatic rings was initiated by forming polycyclic aromatic structures as indicated by the broadening of the C=C stretching band located at 1560/cm. This behavior is in agreement with the published literature [26]. With further condensation of polycyclic aromatic structures at higher carbonization temperatures (700 °C and above), the delocalized aromatic (C=C) stretching peak at 1560/cm disappeared completely (Fig. 8). Only an extremely weakened trace of the delocalized C=C stretching band can be seen in the 700 °C spectrum (Fig. 8b). After the carbonization at 1000 °C, the delocalized C=C stretching band cannot be observed possibly due to the strong absorption of carbon fibers becoming completely invisible

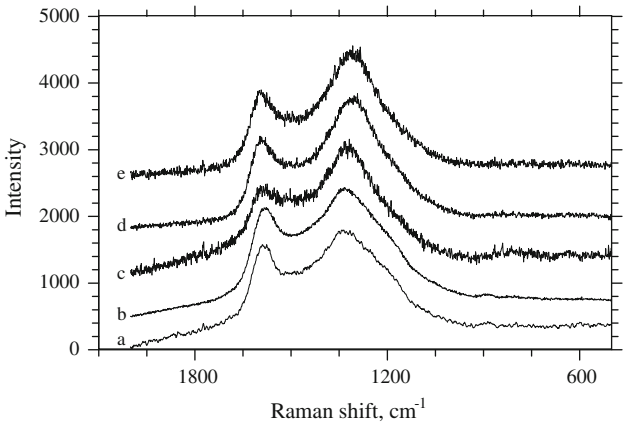


Fig. 9 Raman spectra of carbonized samples as a function of carbonization temperature in the 2000–500/cm range. **a** 600 °C, **b** 700 °C, **c** 800 °C, **d** 900 °C, **e** 1000 °C

arising from the black body radiation of the carbonized viscose rayon fiber [26].

Raman spectroscopy

In recent years, Raman spectroscopy has been successfully used as a non-destructive method to characterize the complex microstructure of carbon-based materials [51]. Raman spectroscopy is also useful for the investigation of structural changes occurring during the carbonization process. The optical penetration depth of the exciting laser used during the collection of Raman spectra is reported to be in the order of 100 nm (for the 488 nm line of Ar^+ laser) [52].

The structure of the carbonized samples was further characterized using Raman spectroscopy. Figure 9 shows the Raman spectra of the samples carbonized in the temperature range 600–1000 °C. The Raman spectra plotted in Fig. 9 are characterized by two predominant first-order bands corresponding to the G- and D-bands [47].

The curve-fitting procedure was carried out to obtain accurate peak parameters for the Raman spectra shown in Fig. 9. Figure 10 illustrates a typical curve fitting of the sample carbonized at 1000 °C for 30 min. The best curve fitting for this sample was performed with three Lorentzian peaks at 1180 (T-band), 1312 (D-band), and 1597 (G-band) /cm and a Gaussian peak at 1515 (D''-band) /cm (Fig. 10) [53].

The G-band is assigned to in-plane vibrations of sp^2-bonded crystalline carbon and has been observed for single crystal graphite [54]. For polycrystalline graphite, however, another peak denoted as the 'disorder' peak (D-band) is typically observed. This band is attributed to in-plane vibrations of sp^2-bonded carbon with structural imperfections (D-band). The D-band is also associated with the

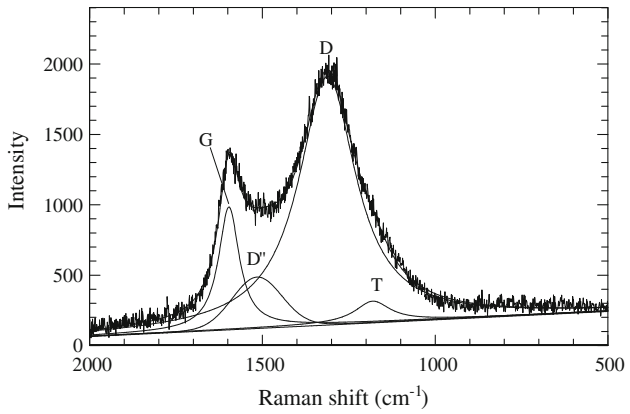


Fig. 10 Curve fitting of Raman spectrum of the sample carbonized at 1000 °C

Table 4 Analysis of Raman spectra obtained from the carbonization of viscose rayon fibers pretreated with combined 3 % (w/v) phosphoric acid (H_3PO_4) and 4 % (w/v) boric acid (H_3BO_3) solution as a function of carbonization temperature

Carbonization temp (°C)	Half-height width (G)	Peak position (G)	Peak position (D)	Half-height width (D)	I_D/I_G
600	91.5	1589	1330	251.2	1.32
700	89.7	1588	1329	249.4	1.46
800	87.6	1594	1323	206.6	1.65
900	72.7	1596	1312	204.2	1.68
1000	69.9	1598	1311	201.0	1.72

disordered and strongly distorted structure of turbostratic carbon and is absent in the Raman spectrum of perfect graphite. The T-band is assigned to sp^3-carbon in the carbonaceous samples. The broad D-band is associated with an amorphous sp^2 carbon bonded in the graphitic phase [53].

The results obtained from the curve fitting of Raman spectra show that the peak position of the G-band increases and its bandwidth (i.e., HHW) decreases with increasing carbonization temperature indicating an increase of order in the carbon structure at higher temperature (Table 4). The full width at half-maximum intensity of the D-band was used as the major parameter to estimate the disorder degree of polyaromatic stacks [55].

As can be seen from Table 4, the HHW of the D-band decreases with increasing carbonization temperature. This behavior is due to the increasing degree of ordering arising from the increase in polyaromatic stack size. The decrease in HHW results from the formation of polyaromatic stacks (layers), destruction of crosslinks occurring between aliphatic and aromatic carbons, and the volatilization of oxygen-containing functional groups during carbonization steps [56].

A parameter often used as a measure of L_a is the ratio of the intensities of D- and G-bands, I_D/I_G. This is due to the fact that G-band intensity may be regarded as a measure of the average volume of the ordered graphite crystals, and the D-band intensity is a measure of the surface area of carbon atoms at the edge of graphitic planes [57]. Thus, analysis of the I_D/I_G ratio provides a measure of the average crystallite thickness. Such an approach has been provided by Tuinstra and Koenig [54], where the I_D/I_G ratio was shown to be inversely proportional to the crystallite thickness, L_a, of graphitic materials.

It is noted from Table 4 that the peak position of the G-band increases from 1588 to 1598/cm with increasing carbonization temperature indicating that more sp^2 carbons are formed at higher temperatures. Table 4 also shows that the intensity ratio of I_D/I_G increases with increasing carbonization temperature. This is typical of the onset of a carbonized structure. As the carbonization temperature is increased, the crystallites consisting of cyclic structures-containing 4 or 5 carbon atoms grow in size and/or number, and this contributes to Raman scatter, causing the I_D/I_G to increase. The I_D/I_G ratio values were observed to increase from 1.32 to 1.72 with progressing carbonization temperature, which is typical of the onset of a carbonized cellulose structure [28]. This behavior is consistent with observations of electrospun cellulose-based carbon nanofibers [28], regenerated liquid crystalline cellulose-based carbon fibers [47], Japanese cedar wood [56], softwood [58], glassy carbons from polyfurfuryl alcohol [59], and carbon aerogels [60], but is in contrast to that observed in PAN-based carbon fibers [61], where the I_D/I_G values were found to decrease with increasing carbonization temperature. The increase in I_D/I_G height ratios indicates that graphene-like structures grow by consuming and re-organizing more amorphous structures as they are exposed to severe thermal treatments [62]. Figure 11 shows the relationship between I_D/I_G height ratios and the average crystallite size (L_a) obtained from X-ray diffraction analysis. It suggests that the increase in the values of I_D/I_G height ratios is related to crystallite size increase in the carbon layer planes (L_a).

Tensile properties

Table 5 shows the tensile properties of oxidized and carbonized viscose rayon fibers pretreated with a combined 3 % (w/v) phosphoric acid (H_3PO_4) and 4 % (w/v) boric acid (H_3BO_3) solution as a function of carbonization temperature. Figure 12 presents the stress-extension at break (%) curves as a function of carbonization temperature. It is clear that the stress-elongation at break curves for the oxidized (250 °C 30 min) and carbonized samples presented in Fig. 12 show an elastic deformation. As

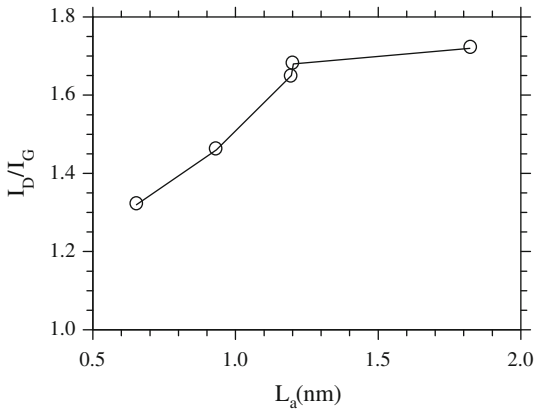


Fig. 11 Comparison of the values of I_D/I_G ratio obtained from the curve fitting of Raman spectra against L_a values obtained from the curve fitting of equatorial X-ray diffraction traces of carbonized viscose rayon fibers in the temperature range 600–1000 °C

expected, the plastic deformation is absent in the tensile curves of the selected carbonized samples (Fig. 12b–d).

The effects of carbonization temperature are clearly identifiable from both Table 5 and Fig. 12. The increasing carbonization temperature from 600 to 1000 °C caused an increase in both tensile strength and modulus values. Tensile strength values increase from 7 to 20 MPa with increasing carbonization temperature. The increase in tensile strength with increasing temperature may be related to the reduction of the size of the surface flaws that cause failure in most cases [63].

The results presented in Table 5 indicate that the tensile modulus of carbonized samples increases along with the temperature. This behavior is caused by the gradual elimination of non-carbon elements in the carbonized samples, which lead to the formation of carbon basal planes.

As mentioned before, a large amount of voids are normally incorporated during the wet spinning of viscose rayon fibers [11]. Thus, the experimental values of tensile modulus were corrected from the effects of porosity using Eq. (3). As shown in Table 5, after porosity correction, the tensile modulus increased from 13.1 to 36.3 GPa. Porosity correction caused an average increase of tensile modulus between 22 and 31 % (Table 5). The formation of carbon basal planes with increasing temperature enhanced the densification of the carbon fibers and promoted the stacking arrangement of carbon basal planes. Therefore, there are a greater number of graphene stacking layers (L_c/d, Table 2), which give rise to improved tensile modulus. The increase in tensile modulus is also related to the molecular orientation of the carbon fibers. It is highly likely that the increasing carbonization temperature caused an increase in the molecular orientation of the carbon structures along the fiber axis, which in turn caused an increase in tensile modulus.

Figure 13 illustrates the relationship between the tensile strength and modulus of the carbon fiber samples. Since the tensile strength-elongation at break values are perfectly elastic at room temperature, the ratio of tensile strength to modulus gives the true elastic strain at fracture. The fracture strain (i.e., elongation at break) for the carbon fiber samples varies between 0.7 and 1 % (Table 5).

Electrical properties

Elongated carbon layer strips containing aromatic carbon layers (graphene layers) are known to be formed during carbonization reactions. The structures of these aromatic carbon layers are in agreement with graphite but less ordered. These structures are called turbostratic graphite and are usually characterized by disordered graphene layers with poor orientation along the fiber axis. Along the direction of the fiber axis containing graphene planes, electrical conductivity may be generated by the movement of π-electrons [64].

The results listed in Table 6 indicate that the resistivity values of the resultant carbon fibers prepared decrease with increasing temperature. Along with the increase in carbonization temperature, the electrical conductivity of the carbon fibers gradually increases.

Due to the elimination of non-carbon elements during the carbonization reactions between 600 and 1000 °C, the

Table 5 Tensile properties of oxidized and carbonized viscose rayon fibers pretreated with combined 3 % (w/v) phosphoric acid (H_3PO_4) and 4 % (w/v) boric acid (H_3BO_3) solution as a function of carbonization temperature

Carbonization temp (°C)	Porosity (%)	Tensile strength (MPa)	Extension at break (%)	Experimental tensile modulus (GPa)	Corrected tensile modulus (GPa)
Untreated	–	300 ± 2	10.6 ± 1.3	9.2 ± 1	–
250 °C 30 min	–	110 ± 2	4.7 ± 1.1	6.1 ± 2	–
600	23.53	7 ± 1	1 ± 0.5	10 ± 2	13.1
700	23.08	9 ± 1	0.7 ± 0.1	16 ± 3	20.8
800	17.88	11 ± 1	0.7 ± 0.1	22 ± 4	26.8
900	18.37	14 ± 2	1.0 ± 0.2	24 ± 3	29.4
1000	20.08	20 ± 2	1.0 ± 0.2	29 ± 4	36.3

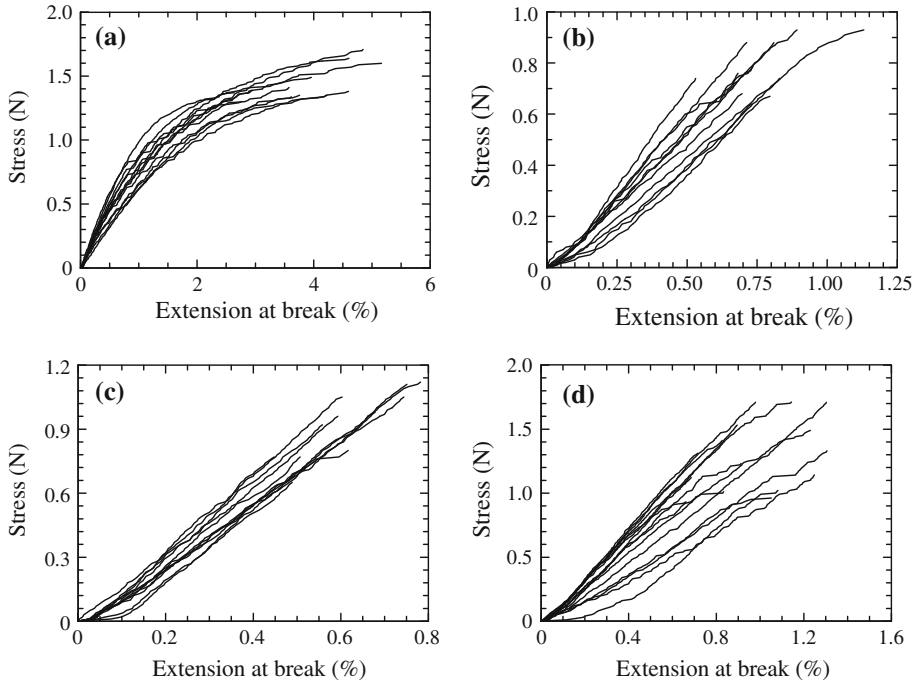


Fig. 12 Stress against extension at break (%) as a function of carbonization temperature. **a** Oxidized at 250 °C 30 min, **b** 600 °C, **c** 800 °C, **d** 1000 °C

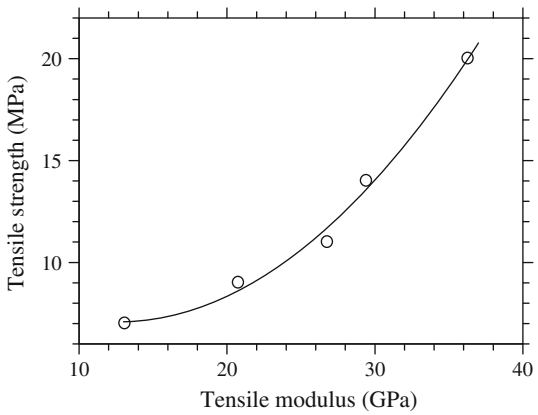


Fig. 13 Relationship between tensile strength and tensile modulus of carbon fiber samples as a function of carbonization temperature

proportion of carbon content increases gradually and a highly conductive graphite-like structure tends to be formed causing a sharp increase in electrical conductivity. The electrical conductivity at a carbonization temperature of 600 °C is found to be 1.65×10^{-7} S/cm and rises sharply to 3.32×10^{-2} S/cm at 1000 °C.

As mentioned above in the discussion of X-ray diffraction results, the apparent crystallite size (L_a) of carbon fibers was found to increase and the interplanar *d*-spacing was found to decrease with progressing temperature. The results suggest that the lateral growth of the graphene-like structures is possibly responsible for the observed increases in the electrical conductivity. Movement of electrons is reported to be most prominent along the hexagonal carbon layers [51].

Due to the turbostratic nature of carbon fibers produced in the present investigation, the electrical conductivity was not found to be as high as in pure graphite (2.5×10^4 S/cm) [65]. To increase the electrical conductivity of carbon fibers prepared in the present investigation to much higher values, carbonization temperatures must also be increased significantly to above 1000 °C, or possibly to 2500 or even to 3000 °C under tension.

Conclusions

The oxidation and carbonization steps of viscose rayon fibers were carried out in the presence of 3 % PA and 4 % BA impregnation. The results showed that PA–BA impregnation improved oxidative stability and hindered the evolution of volatile by-products by blocking the primary hydroxyl groups. During the oxidation step performed at 250 °C, the cellulose II crystalline structure was totally eliminated due to the amorphization reactions caused by the destruction of intramolecular and intermolecular hydrogen bonds. Carbonization was performed in an inert atmosphere at temperatures ranging from 600 to 1000 °C in steps of 100 °C with a residence time of 30 min. The results acquired from the fiber thickness, linear density, carbon fiber yield, elemental analysis, volume density, X-ray diffraction, IR and Raman spectroscopy, tensile properties, and electrical conductivity measurements showed that the carbonization temperature had an influential role on the structure and properties of the resulting carbon fibers.

Table 6 Electrical properties of carbonized fiber samples as a function of carbonization temperature

Carbonization temp (°C)	Resistivity /Ω/cm	Conductivity S/cm	Log (conductivity)
600	$6.06 \pm 1.22 \times 10^{6}$	$1.65 \pm 0.34 \times 10^{-7}$	-6.78 ± 0.06
700	$0.91 \pm 0.37 \times 10^{4}$	$1.10 \pm 0.31 \times 10^{-4}$	-3.96 ± 0.20
800	$5.14 \pm 0.21 \times 10^{1}$	$1.94 \pm 0.27 \times 10^{-2}$	-1.71 ± 0.22
900	$5.05 \pm 0.65 \times 10^{1}$	$1.98 \pm 0.11 \times 10^{-2}$	-1.70 ± 0.24
1000	$3.01 \pm 0.99 \times 10^{1}$	$3.32 \pm 0.49 \times 10^{-2}$	-1.48 ± 0.20

Carbon fibers obtained from oxidized viscose rayon fibers exhibited physical and chemical changes with increasing carbonization temperature. They were characterized by a decrease in fiber thickness and linear density values due to the elimination of non-carbon elements in the form of volatiles such as H_2O, CO, and CO_2 together with increases in the values of carbon content, C/H ratio, volume density, tensile strength, tensile modulus, and electrical conductivity. The results obtained from linear density measurements indicated a carbon fiber yield of 33.7 % at the carbonization temperature of 1000 °C. Elemental analysis of carbon fibers showed that the carbon content increased from 77.5 to 90.2 % whereas the hydrogen content decreased from 2.5 to 0.6 % when carbonization temperature increased from 600 to 1000 °C. C/H ratio was also found to increase with progressing temperature. X-ray diffraction analysis revealed that the interplanar *d*-spacing (d_{002}) decreased, and that the apparent crystallite thickness (L_c) and the apparent crystallite width (L_a) increased with increasing carbonization temperature. Infrared spectroscopy in agreement with the elemental analysis showed the loss of OH, CH, C=O, CH_2, C–O, and C–O–C groups due to the elimination of oxygen and hydrogen atoms caused by the totally completed dehydration and dehydrogenation reactions. The results obtained from X-ray diffraction, IR spectroscopy, and elemental analysis showed that the crystalline cellulose structure was totally lost due to the formation of an amorphous carbon structure during carbonization reactions.

Acknowledgements The assistance and cooperation of KARSU AŞ (Kayseri) is gratefully acknowledged for providing the viscose rayon multifilaments. The financial support of the Scientific Research Projects Unit of Erciyes University is very much appreciated (project number FLY-2013-4770). Thanks are also extended to Prof Dr Mehmet Ari (Department of Physics, Erciyes University) for the electrical conductivity measurements and to Prof Dr Talat Özpozan (Department of Chemistry, Erciyes University) for the Raman spectroscopy measurements.

References

1. Edison TA (1880) Electrical lamp. US Pat. 223,898
2. Frohs W, Jaeger H (2011) Carbon fiber & composite material-landscape Germany. Tanso 249:174–178
3. Johnson W, Phillips LN, Watt W (1966) Production of carbon fibres and compositions containing said fibres. US Pat. 3,412,062
4. Bacon R, Schalamon WA (1969) Physical properties of high modulus graphite fibers made from a rayon precursor. Appl Polym Symp 9:285–292
5. Shindo A, Nakanishi Y, Soma I (1969) Carbon fibers from cellulose fibers. Appl Polym Symp 9:271–284
6. Chand S (2000) Carbon fibers for composites. J Mater Sci 35:1303–1313. doi:10.1023/A:1004780301489
7. Zhang H, Guo L, Shao H, Hu X (2006) Nano-carbon black filled lyocell fiber as a precursor for carbon fiber. J Appl Polym Sci 99:65–74
8. Sevilla M, Fuertes AB (2010) Graphitic carbon nanostructures from cellulose. Chem Phys Lett 490:63–68
9. Dumanlı AG, Windle AH (2012) Carbon fibres from cellulosic precursors: a review. J Mater Sci 47:4236–4250. doi:10.1007/s10853-011-6081-8
10. Wu Q, Pan D (2002) A new cellulose based carbon fiber from a lyocell precursor. Textile Res J 72:405–410
11. Peng S, Shao H, Hu X (2003) Lyocell fibers as the precursor of carbon fibers. J Appl Polym Sci 90:1941–1947
12. Donnet J-B, Wang TK, Peng JCM (eds) (1998) Carbon fibers, 3rd edn. Marcel Dekker Inc, New York, pp 41–64
13. Li H, Yang Y, Wen Y, Liu L (2007) A mechanism study on preparation of rayon based carbon fibers with $(NH_4)SO_4/NH_4Cl$/organosilicon composite catalyst system. Compos Sci Technol 67:2675–2682
14. Ross SE (1968) Observations concerning the carbonization of viscose rayon yarn. Textile Res J 38:906–913
15. Ko YG, Choi US, Kim JS, Park YS (2002) Novel synthesis and characterization of activated carbon fiber and dye adsorption modelling. Carbon 40:2661–2672
16. Sun J, Wu L, Wang Q (2005) Comparison about the structure and properties of PAN-based activated carbon hollow fibers pretreated with different compounds containing phosphorus. J Appl Polym Sci 96:294–300
17. Ayranci E, Hoda N (2005) Adsorption kinetics and isotherms of pesticides onto activated carbon cloth. Chemosphere 60:1600–1607
18. Ayranci E, Hoda N (2004) Adsorption of bentazon and propanil from aqueous solutions at the high area activated carbon cloth. Chemosphere 57:755–762
19. Kadirvelu K, Faur-Brasquet C, Le Cloirec P (2000) Removal of Cu(II), Pb(II), and Ni(II) by adsorption onto activated carbon cloths. Langmuir 16:8404–8409
20. Wu J, Chung DDL (2002) Increasing the electromagnetic interference shielding effectiveness of carbon fiber polymer-matrix composite by using activated carbon fibers. Carbon 40:445–467
21. Xu B, Wu F, Chen S, Zhang C, Cao G, Yang Y (2007) Activated carbon fiber cloths as electrodes for high performance electric double layer capacitors. Electrochim Acta 52:4595–4598
22. Chen Y, Jiang N (2007) Carbonized and activated non-wovens as high-performance acoustic materials: Part I noise absorption. Textile Res J 77:785–791
23. Chen Y, Jiang N (2009) Carbonized and activated non-wovens as high-performance acoustic materials: Part I noise insulation. Textile Res J 79:213–218

24. Alcaniz-Monge J, De la Casa-Lillo MA, Cazorla-Amoros D, Linares-Solano A (1997) Methane storage in activated carbon fibres. Carbon 35:291–297
25. De la Casa-Lillo MA, Lamari-Darkrim F, Cazorla-Amoros D, Lineros-Solano A (2002) Hydrogen storage in activated carbons and activated carbon fibers. J Phys Chem B106:10930–10934
26. Zeng F, Pan D (2008) The structural transitions of rayon under the promotion of a phosphate in the preparation of ACF. Cellulose 15:91–99
27. Moutaud GM, Duflos JL (1967) Process of graphitizing 'Polynosic' regenerated cellulose fibrous textile and resulting fibrous graphite textile. US Pat. 3,322,489
28. Kong K, Deng L, Kinloch IA, Young RJ, Eichhorn SJ (2012) Production of carbon fibres from a pyrolysed and graphitised liquid crystalline cellulose fibre precursor. J Mater Sci 47:5402–5410. doi:10.1007/s10853-012-6426-y
29. Goldhalm G (2012) Tencel carbon precursor. Lenzinger Berichte 90:58–63
30. Kim D-Y, Nishiyama Y, Wada M, Kuga S (2001) Graphitization of highly crystalline cellulose. Carbon 39:1051–1056
31. Kuga S, Kim D-Y, Nishiyama Y, Brown RM Jr (2002) Nanofibrillar carbon from native cellulose. Mol Cryst Liq Cryst 387:237–243
32. Li N, Eichhorn SJ (2006) Potential stiffness of carbon fibres produced from highly crystalline cellulose. J Mater Sci 41:4993–4995. doi:10.1007/s10853-006-0138-0
33. Sharon M, Sharon M, Kalita G, Mukherjee B (2011) Hydrogen storage by carbon fibers synthesized by pyrolysis of cotton fibers. Carbon Lett 12:39–43
34. Worasuwannarak N, Hatori S, Nakagawa H, Miura K (2003) Effect of oxidation pre-treatment at 220 to 270 °C on the carbonization and activation behavior of phenolic resin fiber. Carbon 41:933–944
35. Wu Q-L, Gu S-Y, Gong J-H, Pan D (2006) SEM/STM studies on the surface structure of a novel carbon fiber from lyocell. Synth Mater 156:792–795
36. Huang X (2009) Fabrication and properties of carbon fibers. Materials 2:2369–2403
37. Hindeleh AM, Johnson DJ, Montague PE (1983) Fibre diffraction methods. In: French AD, Gardner KH (eds) ACS Symp. No. 141. American Chemical Society, Washington DC, p 149
38. Ari H, Soykan C, Özpozan T (2013) Preparation of organic/inorganic hybrid materials using aggregates of poly [2-methyl-N[2-(phenylthio)phenyl] acrylamide-co-2-(trimethylsyloxy) ethyl methacrylate] as precursor and vibrational investigation of the polymerization. J Macromol Sci A 50:1022–1041
39. Smits, FM (1958) Measurement of sheet resistivities with the four-point probe. Bell Syst Tech J 37:711–718
40. Erat S, Metin H, Ari M (2008) Influence of the annealing in nitrogen atmosphere on the XRD, EDX, SEM and electrical properties of chemical bath deposited CdSe thin films. Mater Chem Phys 111:114–120
41. Stokes AR (1948) A numerical Fourier-analysis method for the correction of widths and shapes of lines on X-ray powder photograph. Proc Phys Soc A166:382–391
42. Zhang X, Lu Y, Xiao H, Peterlik H (2014) Effect of hot stretching graphitization on the structure and mechanical properties of rayon-based carbon fibers. J Mater Sci 49:673–684. doi:10.1007/s10853-013-7748-0
43. Ruland W (1969) The relationship between preferred orientation and Young's modulus of carbon fibers. Appl Polym Symp 9:293–301
44. Sauder C, Lamon J (2005) Prediction of elastic properties of carbon fibers and CVI matrices. Carbon 43:2044–2053
45. Karacan I, Soy T (2013) Structure and properties of oxidatively stabilized viscose rayon fibers impregnated with boric acid and phosphoric acid prior to carbonization and activation steps. J Mater Sci 48:2009–2021. doi:10.1007/s10853-012-6970-5
46. Langan P, Nishiyama Y, Chanzy H (2001) X-ray structure of mercerized cellulose II and 1 Å resolution. Biomacromolecules 2:410–416
47. Deng L, Young RJ, Kinloch IA, Zhu Y, Eichhorn SJ (2013) Carbon nanofibres produced from electrospun cellulose nanofibers. Carbon 58:66–75
48. Tomizuka I, Isoda Y, Amamiya Y (1981) Carbon fibre from a high-modulus polyamide fibre (Kevlar). Tanso 106:93–101
49. Ko KS, Park CW, Yoon S-H, Oh SM (2001) Preparation of Kevlar-derived carbon fibers and their anodic performances in Li secondary batteries. Carbon 39:1619–1625
50. Puziy AM, Poddubnaya OI, Martinez-Alonso A, Suarez-Garcia F, Tascon JMD (2002) Synthetic carbons activated with phosphoric acid I. Surface chemistry and ion binding properties. Carbon 40:1493–1505
51. Mennella V, Monaco G, Colangeli L, Bussoletti E (1995) Raman spectra of carbon based materials excited at 1064 nm. Carbon 33:115–121
52. Escribano R, Sloan JJ, Siddiqui N, Sze N, Dudev T (2001) Raman spectroscopy of carbon-containing particles. Vib Spectrosc 26:179–186
53. Rhim Y-R, Zhang D, Fairbrother DH, Wepasnick KA, Livi KJ, Bodnar RJ, Nagle DC (2010) Changes in electrical and microstructural properties of microcrystalline cellulose as function of carbonization temperature. Carbon 48:1012–1024
54. Tuinstra F, Koenig JL (1970) Raman spectrum of graphite. J Chem Phys 53:1126–1130
55. Ishimaru K, Hata T, Bronsveld P, Meier D, Imamura Y (2007) Spectroscopic analysis of carbonization behavior of wood, cellulose and lignin. J Mater Sci 42:122–129. doi:10.1007/s10853-006-1042-3
56. Yamauchi S, Kurimoto Y (2003) Raman spectroscopic study on pyrolyzed wood and bark of Japanese cedar: temperature dependence of Raman parameters. J Wood Sci 49:235–240
57. Sze S-K, Siddiqui N, Sloan JJ, Escribano R (2001) Raman spectroscopic characterization of carbonaceous aerosols. Atmos Environ 35:561–568
58. Paris O, Zollfrank C, Zickler GA (2005) Decomposition and carbonization of wood biopolymers-a microstructural study of softwood pyrolysis. Carbon 43(1):53–66
59. Nakamizo M (1991) Raman spectra of iron-containing glassy polymers. Carbon 29:757–761
60. Maldonado-Hodar FJ, Moreno-Castilla C, Rivera-Utrilla J, Hanzawa Y, Yamada Y (2000) Catalytic graphitization of carbon aerogels by transition metals. Langmuir 16:4367–4373
61. Wang Y, Serrano S, Santiago-Aviles JJ (2003) Raman characterization of carbon nanofibers prepared using electrospinning. Synth Met 138:423–427
62. McDonnald-Wharry J, Manley-Harris M, Pickering K (2013) Carbonization of biomass-derived chars and the thermal reduction of a graphene oxide sample studies using Raman spectroscopy. Carbon 59:383–405
63. Plaisantin H, Pailler R, Guette A, Birot M, Pillot J-P, Daude G, Olry P (2006) Ex-cellulose carbon fibres with improved mechanical properties. J Mater Sci 41:1959–1964. doi:10.1007/s10853-006-1297-8
64. Ko T-H, Huang L-C (1998) The influence of cobaltous chloride modification on physical properties and microstructure of modified PAN fiber during carbonization. J Appl Polym Sci 70:2409–2415
65. Johnson W, Watt W (1967) Structure of high modulus carbon fibres. Nature 215:384–386